Geotextiles and Geomembranes xxx (xxxx) xxx

Contents lists available at ScienceDirect

Geotextiles and Geomembranes

journal homepage: www.elsevier.com/locate/geotexmem

Regular Paper

Rational design method for bituminous pavements reinforced by geogrid

Reuber Freire [a,*], Hervé Di Benedetto [b], Cédric Sauzéat [b], Simon Pouget [c], Didier Lesueur [d,e]

[a] Federal University of Pernambuco, Av. Prof. Moraes Rego, 1235 - Cidade Universitária, 50670-901, Recife, PE, Brazil
[b] University of Lyon / ENTPE, Laboratory of Tribology and System Dynamics (LTDS) (UMR CNRS 5513), 3 Rue Maurice Audin, 69518, Vaulx-en-Velin, France
[c] EIFFAGE Infrastructures Research & Innovation Department, Cedex, 8 Rue Du Dauphiné CS74005, 69964, Corbas, France
[d] Afitexinov, Route Du Pont Du Diable, 38110, Cessieu, France
[e] IMT Nord Europe, Institut Mines-Télécom, Univ. Lille, Centre for Materials and Processes, F-59000, Lille, France

ARTICLE INFO

Keywords:
Geogrid
Reinforcement
Design method
Pavement
Bituminous mixtures
Subject classification codes

ABSTRACT

Geosynthetics have been a reinforced solution for pavement structures for more than 80 years and could be effective in extending its service life. There is a lack of consolidated design methods for pavement with this reinforcement. Therefore, this work aims at proposing a new rational design approach for reinforced structures based on the French design method. In this approach, the geogrid contribution was included by improving the fatigue and rutting properties of some layers, using coefficients named k_{maj} and k_{maj_z}. Three hypotheses were considered concerning the condition of an old bituminous layer remaining from rehabilitation works. The first one considered this layer in healthy condition to simulate a new reinforced structure. The second one considered it as cracked and the third one as disintegrated to simulate the design for rehabilitation. Two placement positions and two geogrid-interface conditions (bonded and not bonded) were analyzed. The results indicated that the geogrid was most effective in a completely deteriorated structure and it should be placed in the lowest possible position in the bound layers. This method can be used for any geogrid position within the structure. Lastly, the reinforcement by geogrid allows a reduction of the thickness of the layer above it.

1. Introduction

Geosynthetics have been used for pavement reinforcement since 1937, when a steel mesh was used to reinforce a 2-km long asphalt layer placed on a 10-yrs old cracked concrete pavement on route M21 in the South West of Grand Rapids (Michigan, USA) (Williams 1954). The idea was simply to mimic reinforced concrete as a way to limit the expected crack reflection from the base layer. Although it was observed from the beginning that the placement of the steel reinforcements was quite tricky, this was replicated on several occasions in the USA and then in Canada and the UK. It confirmed that the technology could potentially delay reflective cracking in asphalt layers, as long as three conditions were met: a correct installation could be achieved, a previous treatment of large cracks was performed (crack sealing) and a thick enough asphalt layer was placed. In parallel, it was also observed very soon that the deconstruction of such reinforced pavements was very complicated and that the corrosion of steel wires could lead to the formation of potholes (Smith and Gartner 1962).

In the 1960s, geosynthetics appeared and were rapidly used in pavements as interlayers to delay reflective cracking once saturated in bitumen (Dykes 1980). The solution was initially found to successfully delay reflection cracking and provide additional benefits due to the waterproofing of the underneath structure (Barksdale 1991). However, the US experience showed that they were not so efficient against reflective cracking especially when considering thick asphalt overlays (over ~8–10 cm).

This is why the development of modern geosynthetics, based on geocomposites combining a geogrid and a thin non-woven geotextile came as an optimized solution combining the advantages of both technologies and suppressing their main drawbacks. They are easier to install than steel meshes, although their installation still requires special attention. They are known to be effective for all asphalt thicknesses above 5 cm and the recommended use of glass fibers make them fully recyclable using common milling machines (Lesueur et al., 2021). As a consequence, these systems have become usual solutions to mitigate reflective cracking (Button and Lytton 2007; MTAG 2009; Nguyen et al., 2013b).

If these products have a proven effect on reflective cracking when correctly installed, their effect on the fatigue life of reinforced asphalt mixtures remain a debated issue. The practical interest of studying

* Corresponding author.
E-mail address: reuber.freire@ufpe.br (R. Freire).

https://doi.org/10.1016/j.geotexmem.2023.04.008
Received 18 November 2022; Received in revised form 16 March 2023; Accepted 26 April 2023

fatigue has been illustrated in a field trial on a secondary road with 400 heavy vehicles/day (RD642 in Aude department - Southern France), where the thickness of the reinforced asphalt layer was significantly reduced yet maintaining the same pavement life (Godard et al., 2019). More precisely, it was shown that a structure based on a 2 cm asphalt leveling course, with a reinforcing glassfiber geocomposite and then 6 cm of wearing course, had a similar structural resistance after 20 years as the unreinforced reference section made with 10 cm asphalt base course and the same wearing course (Godard et al., 2019). In other words, the presence of the reinforcement allowed for an 8 cm asphalt thickness reduction (50%). Still, demonstrating this possibility through a rational pavement design is not an easy task. The justification behind the thickness reduction of the field study on RD624 has not been fully detailed and the published information shows that it was essentially based on an improved fatigue life of reinforced beams as measured in a four-point bending mode in controlled stress mode (Godard et al., 1993). A recent study attempted to further refine this approach but still used another experimental method to evaluate the fatigue life (Nguyen et al., 2021). In addition, fitting parameters are needed and have to be experimentally determined by back-calculations from real pavement deformation data, which makes the method very difficult to generalize. Therefore, this method is far from being useable for everyday pavement design.

In parallel, many other studies demonstrate that geocomposites can have a positive impact on the fatigue life of reinforced asphalt mixtures, but they highlight that the results depend strongly on the geometry and test method being used (Chang et al., 1999; Polidora et al., 2019; Kumar et al., 2021). In particular, changing the position of the reinforcement in the tested specimen has a major impact on fatigue life (Polidora et al., 2019; Nguyen et al., 2020). Moreover, the tested geometry is not representative of a real pavement structure. Therefore, using a fatigue test as the basis for pavement design for these systems is very difficult because the testing is done for a position of the geocomposite in a beam that is not necessarily representative of the position of the reinforcement in the real pavement. In other words, it makes it very difficult if not impossible, to study the impact of the geogrid position in the pavement design.

In this context, we propose a new design method for pavements reinforced by geosynthetics that allows for positioning the system at any location in the structure. This completely new approach is based on the French pavement design method and gives results in line with former studies. The benefits, limits and practical consequences of our method are discussed.

2. Principle of French design method for new and rehabilitated pavements without geogrid

The current French pavement design method has been developed in the 1990s and is in use since then (Service d'Etudes Techniques des Routes et Autoroutes, 1994; Corté and Goux 1996). It has been standardized in 1992 as French standard NF P 98–086, which underwent a thorough revision in 2011 with subsequent update in 2021 (NF P 98–086 2021). Nowadays, France is one of the only countries in the World where the construction team can propose alternative solutions to the project design of a road based on a rational calculation following this standard. Proposed solutions are generally accepted by the owner if they allow significant savings yet maintaining a similar or even better service life. The systematic use of pavement design tools in France explains the rapid spread of high modulus asphalt in the 1990s since very significant savings could be obtained with a marked asphalt thickness reduction (Corté 2001). Such a technological leap was recently repeated with the introduction of GB5 by the Eiffage group (Olard 2012), this bituminous mixture is a high-performances asphalt concrete (AC) for road base layer, that meets the requirements of the NF EN 13108–1 (2016). All of this was made possible thanks to the development of the Alizé software in the 1960s as the official design tool (Corté and Goux 1996) and its subsequent broad diffusion to the whole industry in parallel to the training of pavement engineers.

The French pavement design method is based on the elastic homogeneous isotropic multilayer theory of Burmister (1943), from which the stress and strain in each point of the pavement structure can be calculated. Input parameters are therefore.

- The geometry and intensity of the load. In the French standard (NF P 98–086 2021), the reference axle load is a dual-wheel single axle loaded at 130 kN. It generates two circular contact areas of 0.125 m radius each with a distance between centers of 0.375 m and a 0,662 MPa pressure homogeneously spread over the contact surface. Note that this axle load of 130 kN is used in several other European countries and not only in France (Pereira and Pais, 2017). Using a different axle load of say 80 kN (like in the UK or in the USA), would only numerically change the calculated number of allowed loads (NE – see below) and not change the methodology. Thus, the values of the potential thickness reduction proposed in this work would be of course somewhat different with other axle loads.
- The thickness and nature of each layer. Reference values for the elastic constants (tensile modulus and Poisson's ratio) of the constituting materials are given in the standard at a reference temperature of 15 °C (NF P 98–086 2021). In the case of new bituminous materials or products surpassing standard performance, real values can be accepted if properly documented by mechanical tests (NF P 98–086 2021). As far as pavement reinforcement is concerned, the French guide for pavement rehabilitation (IDRRIM 2016), gives values for the reference modulus of old bituminous materials, to be used in pavement renovation design: 2000 and 500 MPa for respectively cracked ("fissuré" in French) and disintegrated ("désagrégé" in French) asphalt mixtures.
- The bearing capacity of the subgrade. In the French standard (NF P 98–086 2021), the minimum value of the modulus for the corresponding class is used for the calculations. Classes of subgrade bearing capacity are labelled PF1, PF2, PF2+, PF3 and PF4 for minimum moduli of respectively 20, 50, 80, 120 and 200 MPa (NF P 98–086 2021).

The traffic is also taken as an input parameter and comes in a second phase of the design. Once stress and strain fields are determined for each layer, the number of allowed reference axle loads NE for the layer is calculated depending on its nature.

- Bituminous layers are exposed to fatigue failure (Service d'Etudes Techniques des Routes et Autoroutes, 1994; NF P 98–086, 2021). The damage is maximal when the tensile stress is maximal. Therefore, the maximum allowable tensile strain $\varepsilon_{t,adm}$ at the bottom of a bituminous layer is calculated to be:

$$\varepsilon_{t,adm} = \varepsilon_6 \times \left(\frac{NE}{10^6}\right)^b \times k_\theta \times k_c \times k_r \times k_s \quad [m/m] \tag{1}$$

where ε_6 and b are the coefficients for the fatigue law of the corresponding bituminous layer, with ε_6 defined as the strain giving a fatigue life of 1 million cycles, b is a negative constant exponent of the fatigue law and k_i are coefficients (Service d'Etudes Techniques des Routes et Autoroutes, 1994; NF P 98–086, 2021); k_θ is a temperature correction coefficient, obtained as the square root of the ratio of moduli at 10 °C and 15 °C, compensating for the fact that the fatigue parameters are measured at 10 °C when the design is made at 15 °C, k_c is a calibration coefficient between 1 and 1.5, permitting to reconcile calculated vs observed pavement lives, k_r is the risk coefficient, taking into account the observed variability of fatigue results in view of the pavement role (structural, urban or low traffic) with a maximum value of 1 for the highest acceptable risk (50%), and k_s is a subgrade coefficient, taking into account the heterogeneities in the subgrade for the layers placed

right above it. It varies between 1/1.2 and 1 and is taken as 1 for PF3 classes and above (NF P 98–086 2021).

- Granular materials (including the subgrade) are exposed to permanent deformation due to vertical stresses, i.e. rutting (Service d'Etudes Techniques des Routes et Autoroutes, 1994; NF P 98–086, 2021). Therefore, the maximum allowable vertical strain $\varepsilon_{z,adm}$ at the top of a granular layer is calculated to be:

$$\varepsilon_{z,adm} = A \times (NE)^{\alpha} \quad [m/m] \tag{2}$$

where A and α are materials parameters taken to be 0.012 and −0.222, respectively, when NE > 250 000 (NF P 98–086 2021).

Equations (1) and (2) are also used in a different form in order to calculate the allowable number of axle loads for respectively, a bituminous layer (NE_t) (equation (3)) or a granular layer (NE_z) (equation (4)).

$$NE_t = \left(\frac{\varepsilon_{t\_adm}}{\varepsilon_6 \times k_\theta \times k_c \times k_r \times k_s}\right)^{1/b} \times 10^6 \tag{3}$$

$$NE_z = \left(\frac{\varepsilon_{z\_adm}}{A}\right)^{\frac{1}{\alpha}} \tag{4}$$

3. Proposed rational design method for bituminous pavements reinforced by geogrids

The proposed method is a two-steps procedure, where the first one follows the existing rational French design method for new pavements (NF P 98–086 2021) and rehabilitation (IDRRIM 2016), described in the previous section. Therefore, the geogrid contribution is not considered in the calculation procedure in the first step. In the second step, the novelty of the proposed method is presented by considering the geogrid contribution in the calculation. The pavement design calculation is carried out in terms of pavement service life, by considering the number of admissible equivalent axle loads (NE). Thus, the total service life of the reinforced structure (NE_{Total}) is equal to the life duration obtained from step one (NE_1), with the additional life obtained in step two, which is due to the geogrid reinforcement contribution (NE_2). However, in the second step, the structure has different characteristics from the one used for the first step calculation. The bituminous layer underneath the geogrid is assumed to be disintegrated after NE_1 cycles and its stiffness is taken as 500 MPa (IDRRIM 2016), and, the layer above the geogrid is considered to be damaged after NE_1 loading cycles.

The main hypothesis assumed in this method is that the geogrid is not affecting the stress/strain distribution. This hypothesis is validated considering the very small strain level in the geogrid (section 4). It is also apparent from the fact that the stiffness of complexes made with two or more layers of asphalt mixtures holding a geogrid, is essentially unchanged as compared to the same complexes without geogrid (Canestrari et al., 2015; Nguyen et al., 2020). Thus, the contribution is essentially included by majoring the fatigue properties of the bituminous layers above it, and increasing the rutting resistance on top of all granular layers. Concerning the fatigue criterion, the coefficient k_{maj} multiplies the fatigue property ε_6 of the upper layer, increasing its fatigue resistance. This coefficient represents the effect of the geogrid reinforcement in the design. Concerning the rutting criterion, the coefficient k_{maj_Z} divides the ε_z loading on the top of the granular layer.

3.1. Case of new pavement

Fig. 1 illustrates the developed rational design method for new pavements.

During step 1 based on the French design method, a numerical elastic calculation is carried out with the structure as presented in Fig. 1 on left illustration, and three strain values are obtained. First, the horizontal strain at the bottom of the upper layer (ε_{t_U1}), then, the horizontal strain at the bottom of the lower layer (ε_{t_L1}), and, finally, the vertical strain at the top of the soil (ε_{z_1}). The number of admissible equivalent axle loads yielded for step 1 (NE_1) is calculated by the fatigue deterioration of the lower layer. Then, NE_1 could be calculated using Equation (3), considering the horizontal strain numerically calculated (ε_{t_L1}), and the fatigue properties at 15 °C and 25 Hz of the lower layer (ε_{6_L}, b_L), as presented in Equation (5). The following calculation from step 1 is the damage (D_G) suffered by the upper layer during this step. In this case, the number of admissible equivalent axle loads for the upper layer (N_G shown in Equation (6)) is calculated using k_{maj} majoring the fatigue properties at 15 °C and 25 Hz of this layer (ε_{6_U}, b_U). Damage is the ratio between NE_1 and N_G as shown in Equation (7).

$$NE_1 = NE_t(\varepsilon_{t\_L1}, \varepsilon_{6\_L}, b_L) \tag{5}$$

$$N_G = NE_t\left(\varepsilon_{t\_U1}, \varepsilon_{6\_U} \times k_{maj}, b_U\right) \tag{6}$$

$$D_G = NE_1/N_G \tag{7}$$

During step 2, a second numerical elastic calculation is carried out with the structure as presented in Fig. 1 (right illustration), by considering the lower layer as disintegrated with a stiffness of 500 MPa. Two strain values are obtained from this calculation: the horizontal strain at the bottom of the upper layer (ε_{t_U2}), and the vertical strain at the top of the soil (ε_{z_2}). The damage is included in the upper layer by decreasing the number of admissible equivalent axle loads by the percentage calculated in Equation (7) in the previous step. Thus, NE_{2t} is the number of admissible equivalent axle loads in the second step considering fatigue failure, and it is obtained according to Equation (8). Moreover, by reducing the lower layer stiffness to 500 MPa, the rutting on the top of the granular layers could occur. Thus, NE_{2z} is the number of admissible equivalent axle loads in the second step considering rutting failure on granular materials, obtained according to Equation (9). Therefore, NE_2

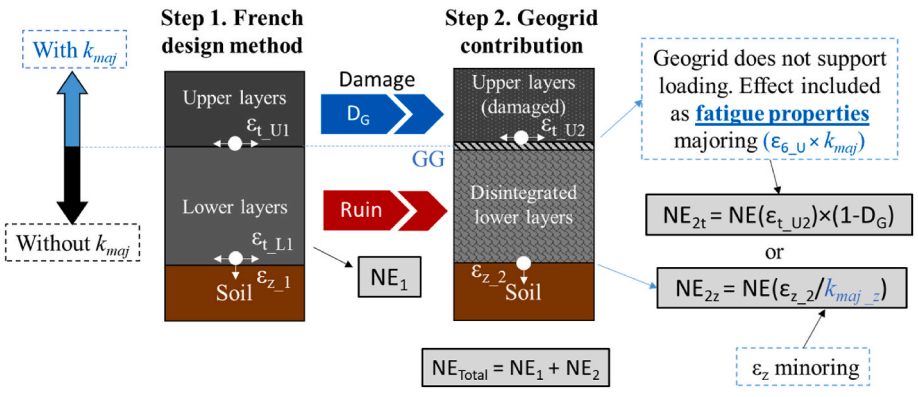

Fig. 1. Principle of proposed design method concerning fatigue properties for the case of construction of new bituminous pavements.

is the smaller value between rutting and fatigue failures (Equation (10)), and is considered the critical parameter for the design.

$$NE_{2t} = NE\left(\varepsilon_{t\_U2}, \varepsilon_{6\_U} \times k_{maj}, b_U\right) \times (1 - D_G) \tag{8}$$

$$NE_{2z} = \left(\frac{\varepsilon_{z\_2}}{A \times k_{maj\_Z}}\right)^{\frac{1}{a}} \tag{9}$$

$$NE_2 = Inf\ (NE_{2t}, NE_{2z}) \tag{10}$$

3.2. Case of rehabilitation of old structures

For rehabilitation of old structures with geogrid reinforcement, the proposed method follows the French rehabilitation method (IDRRIM 2016). In this case, step 1 is divided into steps 1.1 and 1.2, as illustrated in Fig. 2.

During step 1.1, the structure is still capable of resisting a number of equivalent axle loads ($NE_{1.1}$), determined by the fatigue failure on the old layer. It can be calculated using the horizontal strain at the bottom of the old layer (ε_{t_O}), numerically calculated using the structure on the left illustration in Fig. 2, and its fatigue properties at 15 °C and 25 Hz (ε_{6_O}, b_O), as presented in Equation (11). Moreover, damage will occur in both, upper and lower layers, due to the axle loads borne in this step. The horizontal strain at the bottom of the upper layer ($\varepsilon_{t\_U1.1}$) and fatigue properties at 15 °C and 25 Hz (ε_{6_U},b_U) are used to calculate the number of admissible equivalent axle loads for this layer (N_{G1_1}), as presented in Equation (12). Thus, the first damage in the upper layer (D_{G1_1}) is calculated according to Equation (14). Using the horizontal strain at the bottom of the lower layer ($\varepsilon_{t\_L1.1}$) and its fatigue properties at 15 °C and 25 Hz (ε_{6_L},b_L), the number of admissible equivalent axle loads for lower layer is calculated (N_{G1_2}, in Equation (13)). Thus, the damage in the lower layer (D_{G1_2}) is obtained according to Equation (15).

$$NE_{1.1} = NE_t(\varepsilon_{t\_O}, \varepsilon_{6\_O}, b_O) \tag{11}$$

$$N_{G1\_1} = NE_t\left(\varepsilon_{t\_U1.1}, \varepsilon_{6\_U} \times k_{maj}, b_U\right) \tag{12}$$

$$N_{G1\_2} = NE_t(\varepsilon_{t\_L1.1}, \varepsilon_{6\_L}, b_L) \tag{13}$$

$$D_{G1\_1} = NE_{1.1}/N_{G1\_1} \tag{14}$$

$$D_{G1\_2} = NE_{1.1}/N_{G1\_2} \tag{15}$$

During step 1.2, the old layer had its life consumed and is considered to be disintegrated with 500 MPa of stiffness. The previous procedure is similarly carried out again, however, in this case, the number of admissible loads is determined by the smaller value between the fatigue ($NE_{1.2t}$, in Equation (16)) and rutting ($NE_{1.2z}$, in Equation (17)) criteria.

$$NE_{1.2t} = NE_t(\varepsilon_{t\_L1.2}, \varepsilon_{6\_L}, b_L) \times (1 - D_{G1\_2}) \tag{16}$$

$$NE_{1.2z} = NE_z(\varepsilon_{z\_1.2}) \tag{17}$$

Where $\varepsilon_{t\_L1.2}$ is the horizontal strain at the bottom of the lower layer in this step, and $\varepsilon_{z\_1.2}$ is the vertical strain at the top of the soil, numerically calculated using the structure on the center illustration in Fig. 2. Moreover, the upper layer continues to be damaged during the step 1.2. This second damage is obtained using the same procedure of previous calculation, presented in Equations (18) and (19).

$$N_{G2\_1} = NE_t\left(\varepsilon_{t\_U1.2}, \varepsilon_{6\_U} \times k_{maj}, b_U\right) \tag{18}$$

$$D_G = NE_{1.2}/N_{G2\_1} \tag{19}$$

Where $\varepsilon_{t\_U1.2}$ is the horizontal strain at the bottom of the upper layer, also obtained using the structure on the center illustration in Fig. 2.

Lastly, step 2 follows the same procedure as previously described for the new pavements case. The main difference is the existence of two damages to be included in the number of admissible loads for fatigue criterion (NE_{2t}), as presented in Equation (20). Equation (21) presents the number of admissible loads for rutting criterion (NE_{2z}).

$$NE_{2t} = NE_t\left(\varepsilon_{t\_U2}, \varepsilon_{6\_U} \times k_{maj}, b_U\right) \times (1 - D_{G1\_1} - D_G) \tag{20}$$

$$NE_{2z} = NE_z\left(\varepsilon_{z\_2} \,/\, k_{maj\_z}\right) \tag{21}$$

Where ε_{t_U2} is the horizontal strain at the bottom of the upper layer, and is ε_{z_2} the vertical strain at the top of the soil for the second step. They could be obtained from numerical elastic calculation using the structure on the right illustration in Fig. 2.

4. Experimental evaluation of geogrid effect on crack propagation: determination of k_{maj}

Experimental campaign with the four-point bending notched fracture (FPBNF) test, designed at the University of Lyon/ENTPE (Nguyen et al. 2008, 2013a, 2016), was carried out using a single layer and three bi-layered specimens reinforced by geogrid (Freire et al., 2021). The bituminous mixture named BBSG 0/10 (*Béton Bitumineux Semi-Grenu*) was an AC 10 according to the French standards NF EN 13108–1 (2016) composed all tested specimens. The geogrids used to reinforce the bituminous mixtures were Notex Glass® composed of fiberglass yarns knitted to a light polyester veil, with a bituminous coating on both sides. Two types of geogrids were used, with Ultimate Tensile Strength (UTS) of 50 kN/m (C 50/50) and 100 kN/m (C 100/100) in two perpendicular

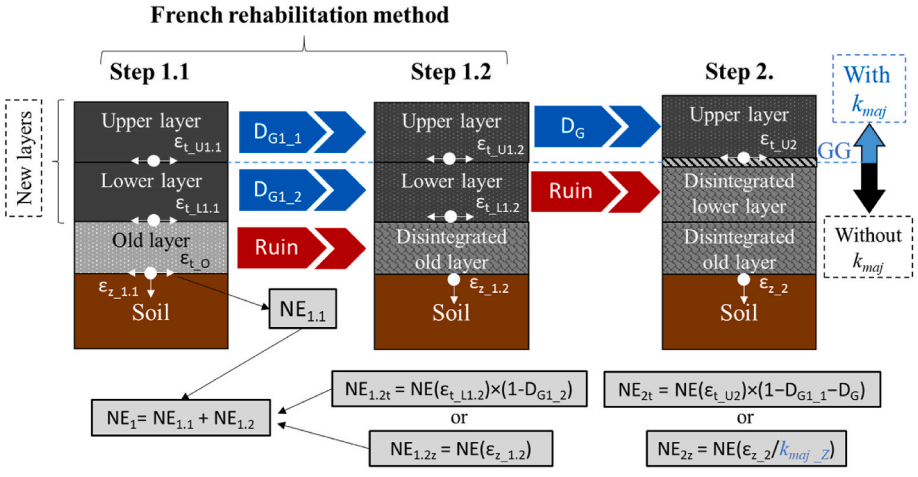

Fig. 2. Principle of proposed design method concerning fatigue properties for the case of rehabilitation of old bituminous pavements.

directions. To bond the geogrid within the interface, a tack coat made with an emulsion of straight run bitumen with 160/220 penetration (NF EN 12591 2009) was used. The specimens with configuration A were made in a single layer, while B, C, and D had interface, considered as "perfectly bonded". Configuration B had only emulsion at a residual binder rate of 290 g/m^2 within the interface. Whereas configurations C and D were made with geogrid (50 and 100 kN/m of UTS) and emulsion at a residual binder rate of 800 g/m^2 applied in two steps. Table 1 presents the details concerning the tested specimens.

Concerning the specimens' fabrication, four slabs were compacted and from each one, prismatic bars, with dimensions 550 mm long, 70 mm wide, and 110 mm deep were sawn. Moreover, a 20 mm deep, 1 mm wide notch was made in its center-bottom. Finally, to perform DIC analysis, a speckle pattern was applied on the rectangular area located in the central length of the beam, with a thin layer of white acrylic paint and a spray of black paint on it. The fabrication procedure is illustrated in Fig. 3(a). The tests were carried out at −5 °C with a monotonic loading at a constant rate of actuator displacement of 0.2 mm/min. Three Linear Variable Differential Transducers (LVDT) were placed on the beam to calculate the deflection, the specimen surface temperature was measured using one thermal gauge (PT100 temperature probe) fixed on the surface and two cameras (CCD Pike F–421 B/C) were used to perform DIC analysis (Fig. 3(b)). All experimental details can be found at Freire et al. (2021).

Fig. 4(a) presents the result of evolution of the crack tip height (a) as a function of the beam deflection for unreinforced specimens A (no interface) and B (interface with straight run bitumen tack coat). The test yielded similar evolution of crack tip height for both configurations. Fig. 4(b) presents the results for unreinforced specimens and includes also the results obtained in the tests conducted with specimens of configuration C (100 kN/m and straight run bitumen tack coat). The crack retarding effect was observed for most of the beams since they presented more deflection before crack propagation from the interface to the upper layer with an increase of 50%. The last one, Fig. 4(c) presents again the results of unreinforced specimens and at this time including the results obtained in the tests conducted with specimens of configuration D (50 kN/m and straight run bitumen tack coat). The deflection measured in the tests of D specimens was approximately 40% higher than unreinforced specimens when the crack reached the interface level. More details and further analysis can be found in Freire et al. (2021).

The results corroborate that geogrid reinforcement is an effective solution to delay reflective cracking in pavements, in accordance with most of the studies in the literature. More precisely, it shows the geogrid capacity to delay crack coalescence in the upper layer. For this reason, it is reasonable to choose the value of 1.4, which is the minimum of the strain ratio values obtained (Fig. 4), for the coefficient k_{maj} considered in the design method. Interestingly, this value is consistent with a former estimate by Van Rompu et al. (2017) based on a different method. Still, further investigation should be conducted to validate this value, which is of course depending on the used geogrid. Concerning k_{maj_z}, the value of 1, meaning it has no effect, was chosen in this work and specific investigation should be done in order to better quantifying this parameter.

Table 1
Tested specimens composition and air voids in bituminous mixtures.

Configuration	Specimen	Interface		Air Voids (in bituminous mixture layers) (%)
		Composition	Tack coat rate (residual binder)	
A	A2-B2	Not applicable	Not applicable	6.3
	A2-B3			7.8
B	B1–B2	Straight run bitumen	292 g/m^2	5.4
C	C3–B1	Straight run bitumen and GG 100 kN/m	2 × 400 g/m^2	6.2
	C3–B2			4.1
	C3–B3			4.7
D	D1-B2	Straight run bitumen and GG 50 kN/m		6.1
	D1-B3			4.3

5. Application of the proposed method on a highway structure

A French highway structure was used for this design method application. This highway was rehabilitated in 2012 as described in Gaborit (2015) and the structure is presented in Fig. 5. BB, GB4 and GB3 are types of French bituminous mixtures belonging to the AC type (NF EN 13108–1 2016), and GRH, GNT2 and PF4 are granular materials (NF P 98–086 2021). During rehabilitation works, some old layers were removed down to the GB3 level, then, two GB4 layers with 8 cm thickness each and one BB with 3 cm thickness were built over it.

Application considers two geogrid placement positions in the new layers: Position 1, between GB4_2 and GB3; and Position 2, between GB4_1 and GB4_2 (see Fig. 5). Moreover, three hypotheses were assumed regarding the GB3 layer condition. Hypothesis A considered the GB3 as a new layer, thus, it represented the design method application for the construction of new pavement reinforced by geogrid. Thus, the GB3 stiffness was assumed as 9300 MPa (NF P 98–086 2021). Hypothesis B and C considered GB3 as deteriorated in different levels, which represented the application for the rehabilitation case. In hypothesis B, GB3 was considered as cracked (partly deteriorated) and the stiffness of this layer was assumed as 2000 MPa. GB3 is disintegrated in hypothesis C (having a stiffness assumed as 500 MPa). Those stiffness values for the layer condition are given by the French rehabilitation method (IDRRIM 2016). Lastly, the interface conditions between all layers were considered as "bonded" during step 1. During step 2, another calculation was included by considering the geogrid interface as "not bonded" (slipping). This last hypothesis of perfect sliding at the interface appears as very severe but may exist in pavement structure. A crack can appears at the interface along the geogrid as observed in some practical cases. The combination of two geogrid positions with three GB3 layer condition hypotheses resulted in 6 studied configurations, illustrated in Fig. 5.

For each studied configuration, a numerical calculation was performed using the Alizé-LCPC software (Corté and Goux 1996). As explained in section 2, Alizé is a multilayer software used in the French design method for new pavements that simulates the stress and strain fields in all layers by considering the materials behaviouras linear elastic and isotropic. The reference load was set as "French standard dual-wheel", which has 0.375 m of wheel spacing, 0.125 m of radius, and 0.662 MPa of pressure.

As INPUT for each layer, material stiffness at 15 °C and 10 Hz, and Poisson's ration (ν) were set as shown in Table 2. Table 3 presents the parameters and constants used for the calculation of the number of admissible equivalent axle loads for fatigue (Equation (3)) and rutting criteria (Equation (4)).

5.1. Case of new pavement construction (hypothesis A)

In hypothesis A, all the layers were considered as new and the stiffness of GB3 was 9300 MPa during step 1. Fig. 6 presents the illustrations of the modelled structures for numerical calculation in steps 1 and 2 for both geogrid positions, between GB4_2 and GB3 (position 1), and between GB4_1 and GB4_2 (position 2).

In numerical simulation using the structure of step 1 of position 1, the horizontal strain at the bottom of GB3 was noticed to be the critical design point, since it defines the smaller number of admissible equivalent axles for fatigue design criterion (NE_{1t}). The vertical strain at the top of GRH, GNT2, and PF4 were obtained, and each one defines a number of admissible equivalent axles for rutting (NE_z). The smaller NE_z obtained for these granular layers was the one for GRH (1.6 E+09), thus, it

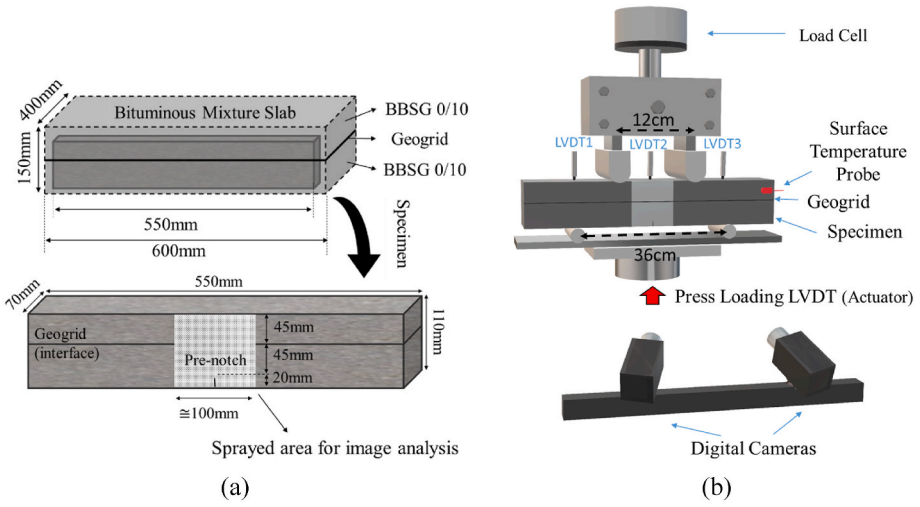

Fig. 3. Illustrations of experimental Four Points Bending Notched Fracture (FPBNF) test (Freire et al., 2021): (a) detail of beam specimen position from the slab, obtained from sawing and prepared for testing, (b) test device and measurement transduces location.

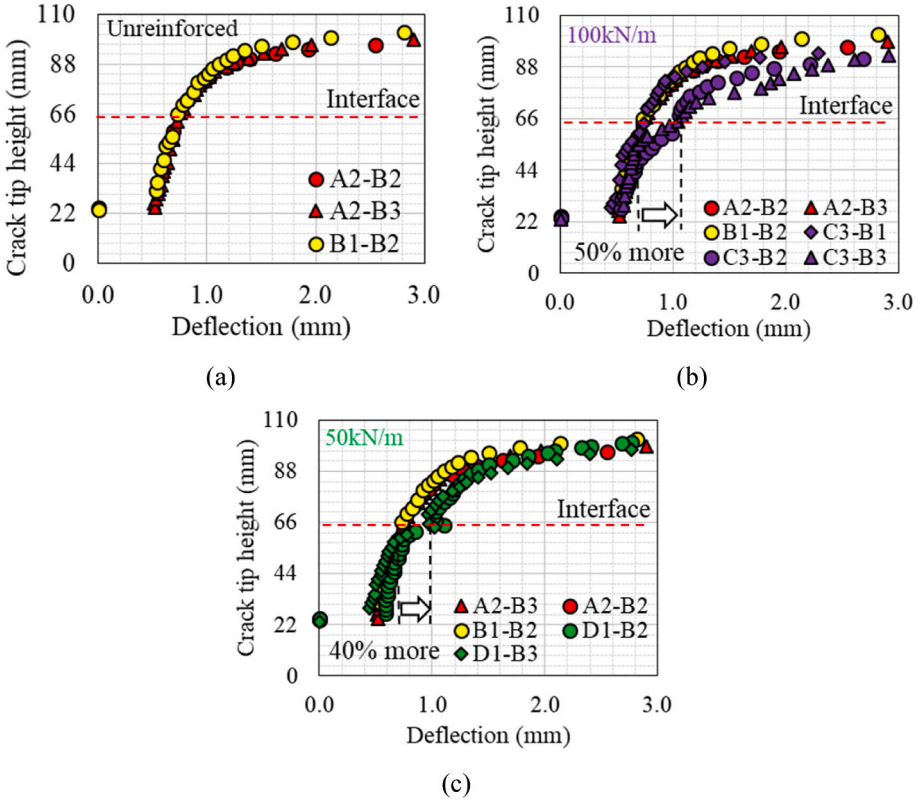

Fig. 4. Crack tip height (from Digital Image Correlation) versus beam deflection (Freire et al., 2021): (a) unreinforced configurations containing interface (B) and no interface (A), (b) configurations A and B including C (geogrid of 100 kN/m), and (c) configurations A and B including D (geogrid of 50 kN/m).

determined NE_{1z}. Lastly, the horizontal strain at the bottom of GB4_2 was measured to calculate the damage occurring in this layer during step 1. These simulated strains and numbers of admissible equivalent axles were calculated using $k_{maj} = 1.4$ (for GB4_2) and $k_{maj\_z} = 1$ (for GRH, GNT2, and PF4), and they are presented in Table 1A in the appendix.

Concerning the step 2, GB3 fatigue life was consumed and the numerical simulation was carried out using the value of 500 MPa as GB3 stiffness. In this case, the horizontal strain at the bottom of GB4_2 determined the number of admissible equivalent axles for fatigue design criterion (NE_{2t}). Once again, the vertical strain at the top of GRH, GNT2, and PF4 were obtained for defining the number of admissible equivalent axles for rutting design criterion (NE_{2t}), which occurred in GRH once again. The strains simulated numbers of admissible equivalent axles using the same previous majoring coefficients are also presented in Table 1A in the appendix.

From the results presented in Table 1A in the appendix, the fatigue in the bituminous mixtures layers should appear much faster than the rutting in granular materials for both steps, even considering $k_{maj\_z} = 1$. Thus, the fatigue was the criterion that controlled the design in this structure. Moreover, the damage occurring in GB4_2 during step 1 was 0.3%, which could be considered as negligible, and the ε_6 majoring of this layer has contributed to that.

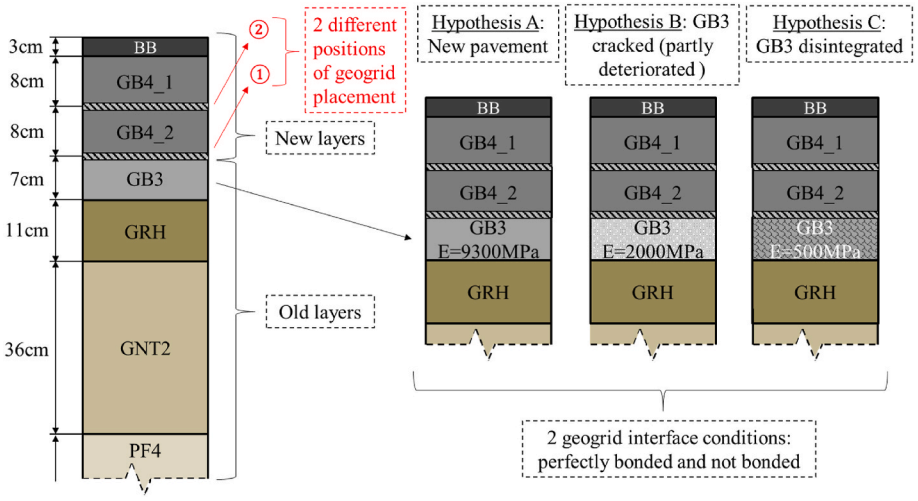

Fig. 5. Considered Highway structure and 6 studied configurations (two different geogrid positions and three GB3 layer conditions).

Table 2
Modulus at 15 °C, 10 Hz and Poisson's ratio for each layer.

Layer	E (15 °C, 10 Hz) (MPa)	ν
BB	5400	0.35
GB4	11 000	0.35
GB3	9300/2000/500	0.35
GRH	400	0.35
GNT2	400	0.35
PF4	200	0.35

Table 3
Fatigue, rutting parameters and design constants for GB3, GB4, BB, and granular layers following the French standards (NF P 98–086 2021).

	GB3	GB4	BB	Granular Layers
ε_6 (10 °C and 25 Hz) (μm/m)	90	100	150	–
b (10 °C and 25 Hz)	−0.2	−0.2	−0.2	–
E (10 °C, 10 Hz) (MPa)	12 300	14 300	7200	–
K_θ	1.15	1.14	1.15	–
Kc	1.3	1.3	1.1	–
Kr	0.84	0.84	0.86	–
Ks	1.00	1.00	1.00	–
A	–	–	–	0.0225
α	–	–	–	−0.244
k_{maj}	1.4	1.4	1.4	–
k_{maj_z}	–	–	–	1

Regarding the position 2, geogrid placed between GB4_1 and GB4_2, the same calculation method was repeated. According to the French design method (Lesueur et al., 2021) used in step 1, when GB3 reaches its fatigue life, the structure is considered as failed. Thus, it was determined by the horizontal strain at the bottom of GB3 (same value obtained for position 1). Then, all the layers below the geogrid position were considered disintegrated (with 500 MPa stiffness) in the second step. The damage in GB4_1 was calculated using the horizontal strain at the bottom of the layer, and majoring the ε_6 by k_{maj}. During step 2, a new simulation was carried out and the horizontal strain at the bottom of GB4_1 determined NE_{1t}. Concerning rutting criterion, for both steps, the vertical strain at the top of GRH, GNT2, and PF4 were obtained and NE_{1z} and NE_{2z} were calculated. Table 2A from appendix presents the results obtained for position 2.

Once again, the fatigue criterion was the critical one for the design, since the number of admissible equivalent axles for fatigue (NE_t) was systematically smaller than for rutting (NE_z).

Lastly, NE_{Total} for position 1 was approximately 2.7 times higher than the one obtained for position 2, considering the geogrid interface as bonded in step 2, and approximately 1.7 times higher considering as not bonded. This result indicates that if the geogrid is placed close to the pavement surface, it decreases the reinforcement potential to extend pavement service life.

5.2. *Case of old pavement structure rehabilitation (hypotheses B & C)*

5.2.1. *GB3 cracked (partly deteriorated, hypothesis B)*

In first studied rehabilitation case, it was assumed that the old layer was partly deteriorated, but still capable of resisting to a certain number

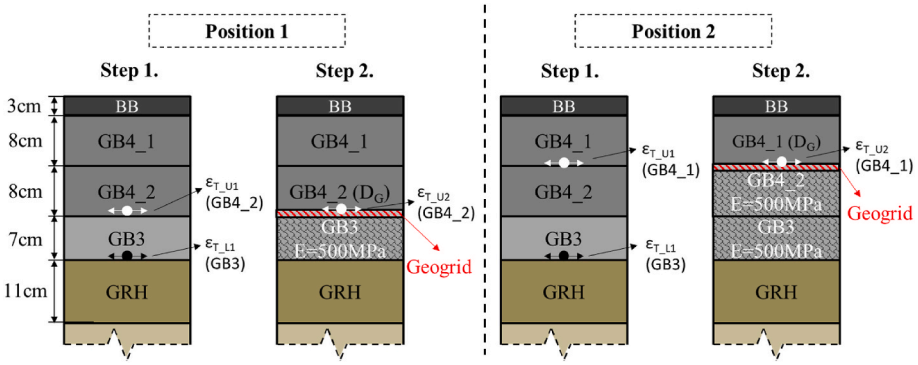

Fig. 6. Modelled structures considering the GB3 as new (E_{GB3} = 9300 MPa) and the two different geogrid positions.

of equivalent axles loads. The deterioration was included as a decrease in GB3 stiffness to the value of 2000 MPa (hypothesis B), corresponding to a cracked layer in the French pavement rehabilitation guide (IDRRIM 2016). This decrease in stiffness raises the strain amplitude in this layer as compared to Hypothesis A, which "consumes" faster the fatigue life of the layer. Fig. 7 presents the modelled structures for numerical simulation, regarding the two geogrid positions studied.

When the geogrid was in position 1, the design calculation follows the same procedure previously done for the case of new pavements. In step 1, the fatigue life was consumed faster than the rutting in the granular layers, and it determined NE_1, which is presented in Table 3A from appendix. In step 2, the simulation was indeed the same as done for the new pavement (hypothesis A - step 2 of position 1). There was still a slight variation in NE_{2t}, since in the rehabilitation case (hypothesis B, step 2 of position 1) the GB4_2 was slightly more damaged than in the previous case (1.8%, presented in Table 3A from appendix). These strains simulated and numbers of admissible equivalent axles calculated using of $k_{maj} = 1.4$ (for GB4_2) and $k_{maj\_z} = 1$ (for GRH, GNT2, and PF4) are also presented in Table 3A from appendix.

In position 2, as mentioned before, the step 1 was divided in 1.1 and 1.2, and for both, the concept from French rehabilitation method was used (IDRRIM 2016). In step 1.1, the $NE_{1.1t}$ was again defined by the fatigue consumption of the GB3 old layer, just as previously calculated in step 1 of position 1. In step 1.2, the GB3 old layer was consumed and the horizontal strain at the bottom of GB4_2 and the damage of 9.8%, calculated in step 1.1 determined $NE_{1.2t}$. The rutting criteria were not critical for the design calculation in step 1.2, since $NE_{1.2z}$ obtained for all granular layers were smaller than $NE_{1.2t}$. Lastly, in step 2, the horizontal strain at the bottom of GB4_1 determined NE_{2t}, and this value was calculated reducing the damages calculated in the two previous steps and using $k_{maj} = 1.4$. Once again, the fatigue was the critical criterion to the design, since NE_{2t} was reached much faster than NE_{2z} of all granular layers. Table 4A from appendix presents all the results obtained and calculated concerning the position 2 of this rehabilitation case (hypothesis B).

Similar to the previous calculation case, the fatigue criterion predominated in relation to the rutting criterion. Moreover, NE_{Total} for position 1 was approximately 3.3 times higher than the one obtained for position 2, considering the geogrid interface as bonded in step 2, and approximately 1.6 times higher considering as not bonded. This result leads to the same conclusion previously made concerning the geogrid position.

5.2.2. GB3 disintegrated (completely deteriorated, hypothesis C)

In the last rehabilitation hypothesis, GB3 layer was considered as completely deteriorated, having 500 MPa of stiffness. This case was included to simulate the rehabilitation of a highly deteriorated pavement. Fig. 8 presents the structures used for numerical simulation for the two geogrid positions. For this calculation, it was assumed that GB3 layer was no longer able to resist to any supplementary axle load. Thus, for step 1 of position 1, NE_{1t} was equal to zero, and, consequently, NE_1 was determined by the fatigue criterion (equal to zero as well). For step 2, the horizontal strain at the bottom of GB4_2 determined NE_{2t}, which was the smaller comparing to NE_{2z} calculated for the granular layers. NE_2 was equal to NE_{2t}, since there was no damage occurring in GBR_2 in step 1. Table 5A from appendix presents all strains simulated and numbers of admissible equivalent axles calculated using of $k_{maj} = 1.4$ (for GB4_2) and $k_{maj\_z} = 1$ (for GRH, GNT2, and PF4).

For the geogrid was placed between GB4_1 and GB4_2 (position 2), during step 1, the layer underneath the geogrid (GB4_2) was consumed by fatigue. Thus, the horizontal strain at the bottom of GB4_2 determined NE_{1t}, and the horizontal strain at the bottom of GB4_1 was used to calculate the damage occurring in this layer during step 1. During step 2, the horizontal strain at the bottom of GB4_1 determined NE_{2t}, and since the damage was negligible (0.004%), it was equal to NE_2. All results regarding position 2 are presented in Table 6A from appendix.

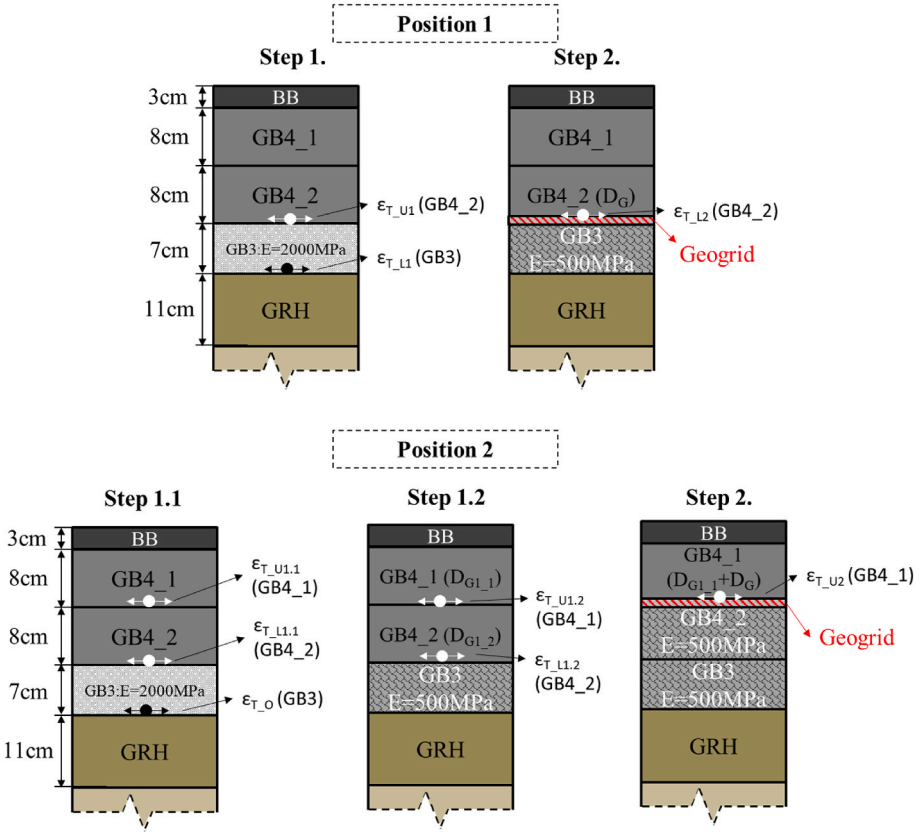

Fig. 7. Modelled structures considering GB3 as cracked (E_{GB3} = 2000 MPa) and the two different geogrid positions.

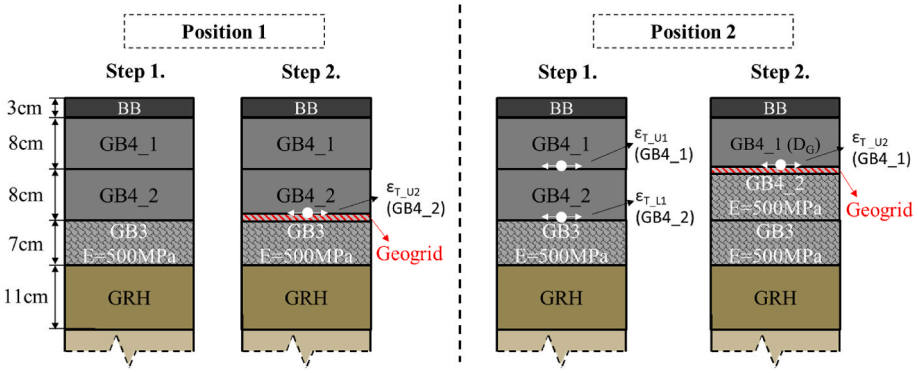

Fig. 8. Modelled structures considering GB3 as disintegrated (E_{GB3} = 500 MPa) and two different geogrid positions.

In this last rehabilitation case, once again the fatigue of the bituminous layers was critical to the design, having all NE values smaller than those obtained for granular layers, even considering $k_{maj\_z} = 1$. For the third time, NE_{Total} for position 1 was higher than the one obtained for position 2 (approximately 3.7 times considering the geogrid interface as bonded in step 2, and approximately 1.7 times higher considering as not bonded). Fig. 9 presents the graphic comparing NE_{Total} calculated using the proposed method for the two studied geogrid placement positions, the two geogrid interface conditions, and the unreinforced case, for the three hypothesis chosen. The unreinforced case was calculated using the classical French method for new pavements (GB3 new) and rehabilitation (GB3 cracked and disintegrated).

The result presented in Fig. 9 shows that the geogrid reinforcement potential changes dramatically depending on its position in the pavement structure. For geogrid position rising towards the pavement surface, NE_{Total} tends to be closer to the NE obtained for unreinforced case, losing the reinforcement ability. Therefore, the geogrid needs to be placed in the lowest possible position in the bound layers (bituminous mixtures layers) of a pavement structure. Table 4 presents the ration between NE_{Total} and NE for unreinforced case, named reinforcement factor, for the three hypotheses concerning GB3 condition and the two studied geogrid positions.

This factor represents the increase in pavement service life due to the reinforcement. This result indicates that for the pavement structure completely deteriorated (hypothesis C, GB3 disintegrated) the geogrid reinforcement was most effective. In this condition and placing the geogrid in position 1, the pavement service life was 5.4 times higher than the life of an unreinforced structure, for bonded geogrid interface in step 2, and 1.9 times higher for not bonded.

Table 4
Reinforcement factors (NE ratio with and without geogrid) obtained for the three GB3 conditions, the two geogrid positions and the two geogrid interface conditions.

Reinforcement factor	GB3 new	GB3 cracked	GB3 disintegrated
Position 1 - Bonded	3.2	4.4	5.4
Position 1 - Not bonded	1.8	1.8	1.9
Position 2 - Bonded	1.2	1.3	1.4
Position 2 - Not bonded	1.1	1.1	1.2

5.3. *Example of application: thickness reduction due to the geogrid reinforcement*

Based on the previous calculations, the geogrid reinforcing a new pavement could extend the pavement service life with a ratio ranging from 1.7 to 3.2 when placed in position 1. This life extension can be equivalent, and, then, transformed in reduction of the structure thickness. Therefore, this application aims at finding a geogrid-reinforced structure with a smaller GB4 thickness that would be able to support the same NE than an unreinforced structure. The GB3 layer condition was considered as new for this calculation and the stiffness used in the numerical simulation was 9300 MPa for this layer. Fig. 10 presents the two structures used for numerical calculation. The unreinforced one was called “reference”. During this application, two conditions were carried out for the reinforced structure: bonded and not bonded. The thickness of the GB4 layer is fitted in order the three calculations (unreinforced and reinforced bonded or not) give the same life duration (same NE). It gives a GB4 layer having 12.1 cm of thickness with geogrid interface considered as perfectly bonded, and a GB4 layer having a thickness of 14 cm with geogrid interface not bonded during step two.

The reference structure NE calculation followed the French design method, thus, the horizontal strain at the bottom of GB3 determined NE_t.

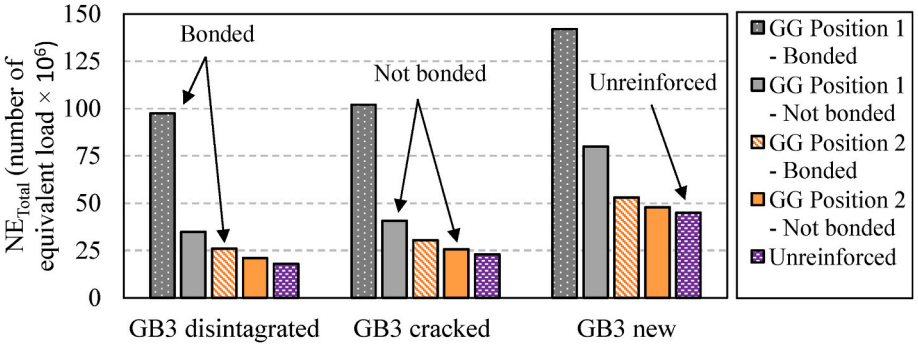

Fig. 9. Total number of admissible equivalent axles (NE_{Total} in million) obtained using the proposed method for the two geogrid positions, for the two geogrid interface conditions, for rehabilitation and new construction with the result obtained for the classical French method for unreinforced structure.

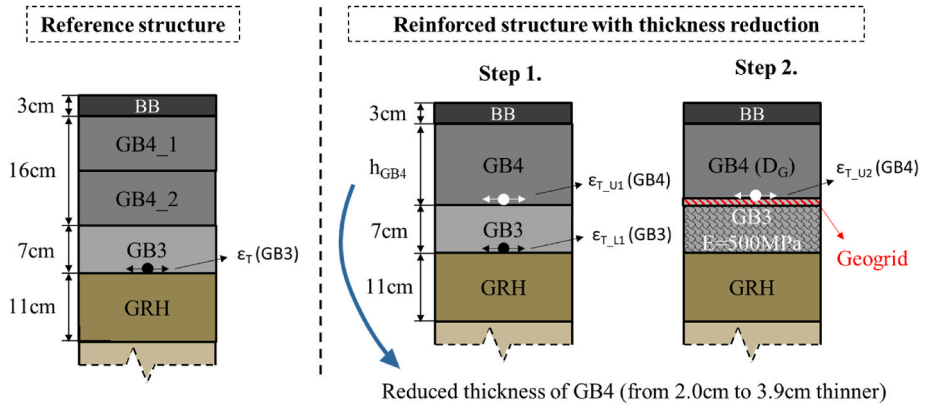

Fig. 10. Reference pavement structure (left) and calculated reinforced with geogrid structure (right) having the same admissible equivalent axles (NE) but reduced GB4 thickness (h_{GB4}). Proposed design method leads to a reduction of 2.0 cm (not bonded case) and 3.9 cm (bonded case).

The NE_z was verified using the vertical strain calculated at the top of the granular layers, and all of them were smaller than NE_t. Concerning the reinforced structure, the calculation procedure was the same for hypothesis A (GB3 new) and position 1, previously presented in this work. The results concerning reference and reinforced structures, for both geogrid interface conditions (bonded and not bonded), are presented in Table 7A from appendix.

As required, the three structures have the same fatigue life. They are able to support 45 million equivalent axles' loads. In addition, the fatigue criterion was the critical one for this type of structure. Therefore, from the proposed design method, the geogrid reinforcement led to a reduction of 3.9 cm of GB4 thickness for the bonded case, representing about 24% reduction, which could significantly reduce the pavement construction costs. This reduction in thickness is of the same order of magnitude as that obtained by considering high performance materials as a replacement for GB4. For example, considering a GB5 asphalt mix (Olard 2012) with the following characteristics, the thickness gain is of 3.6 cm: E (15 °C, 10 Hz) (MPa): 14 000; ν: 0.35; ε_6 (10 °C and 25 Hz): 130; b (10 °C and 25 Hz): 0.2; E (10 °C, 10 Hz) (MPa): 18 150; K_θ: 1.14; Kc: 1.3; Kr: 0.84; and Ks: 1.00. Lastly, concerning not bonded case, the geogrid reinforcement would led to a reduction of 2.0 cm of GB4 thickness, representing more than 10% reduction.

6. Conclusions

This work presented a new design method for pavement structures reinforced by geogrid based on the French design method for new pavements and rehabilitation. In this method, the geogrid effect is taken into account with only two constants k_{maj} and k_{maj_z} depending on the geogrid type. Moreover, this work presented the application of the method in a real pavement structure from a French highway. The main conclusions of this work are presented hereafter.

- The proposed method is simple and takes into account the design criteria for fatigue of bituminous mixture and rutting of granular layers in geogrid-reinforced structures. In addition, this method can be used for any geogrid position within the structure.
- The design uses a majoration coefficient k_{maj} that characterizes the ability of the geogrid to delay crack propagation. It can be determined experimentally using a crack propagation test (Freire et al., 2021) and was found to be 1.4 for the tested geogrids.
- The majoration coefficient k_{maj_z} that characterizes the ability of the geogrid to impact the rutting resistance of the underneath granular layers, was taken as 1 (i.e. no effect). Even if it had a limited effect in our calculations because rutting was never the critical design criterion, this conservative approach will have to be further investigated in future works.
- For fatigue design criterion, the geogrid should be place as low as possible within the bituminous layers. The geogrid reinforcement potential decreases when placed closer to the surface. This result was expected based on the accumulated experience (Button and Lytton 2007; Lesueur et al., 2021; Nguyen et al., 2013b) but it is the first time to our knowledge that the impact of geogrid position can be easily quantified in terms of pavement life
- For the studied French highway structure, the fatigue criterion of bituminous mixtures was always the critical one when comparing to the rutting criterion of granular layers.
- The reinforcement by geogrid allows a reduction of the thickness of the layer above it. This thickness reduction that can be obtained from the developed design method results in a reduction of construction costs

This work, which presents a new design method based on a rational approach, obviously needs further validation and investigation.

Data availability

No data was used for the research described in the article.

Appendix

Table 1A
Numerical calculation results, considering GB3 as new (E_{GB3} = 9300 MPa) and geogrid placed between GB4_2 and GB3

Position 1: Geogrid between GB4_2 and GB3		Layer				
		GB4_2	GB3	GRH	GNT2	PF4
Step 1	ε_t: bottom of layer (μm/m)	25	53	–	–	–
	NE_{1t}	–	4.5 E+07	–	–	–
	N_G	1.7 E+10	–	–	–	–

(continued on next page)

Table 1A (*continued*)

Position 1: Geogrid between GB4_2 and GB3			Layer				
			GB4_2	GB3	GRH	GNT2	PF4
	Damage D_G		0.3%	–	–	–	–
	ε_z: top of layer (μm/m)		–	–	129	103	95
	NE_{1z}		–	–	1.6 E+09	3.9 E+09	5.4 E+09
Step 2 - bonded	ε_t: bottom of layer (μm/m)		70	–	–	–	–
	NE_t		9.7 E+07	–	–	–	–
	$NE_{2t} = NE_t \times (1 - D_G)$		9.7 E+07	–	–	–	–
	ε_z: top of layer (μm/m)		–	–	167	134	118
	NE_{2z}		–	–	5.3 E+08	1.3 E+09	2.2 E+09
Step 2 - not bonded	ε_t: bottom of layer (μm/m)		86	–	–	–	–
	NE_t		3.5 E+07	–	–	–	–
	$NE_{2t} = NE_t \times (1 - D_G)$		3.5 E+07	–	–	–	–
	ε_z: top of layer (μm/m)		–	–	109	120	152
	NE_{2z}		–	–	3.1 E+09	2.1 E+09	7.9 E+08
Total	NE_1		4.5 E+07				
	Bonded	NE_2	9.7 E+07				
		NE_{Total}	1.4 E+08				
	Not bonded	NE_2	3.5 E+07				
		NE_{Total}	8.0 E+07				

Table 2A
Numerical calculation results, considering GB3 as new (E_{GB3} = 9300 MPa) and geogrid placed between GB4_1 and GB4_2

Position 2: Geogrid between GB4_1 and GB4_2			Layer				
			GB4_1	GB3	GRH	GNT2	PF4
Step 1	ε_T: bottom of layer (μm/m)		4	53	–	–	–
	NE_{1t}		–	4.5 E+07	–	–	–
	N_G		1.6 E+14	–	–	–	–
	Damage D_G		0.00003%	–	–	–	–
	ε_z: top of layer (μm/m)		–	–	129	103	95
	NE_{1z}		–	–	1.6 E+09	3.9 E+09	5.4 E+09
Step 2 - bonded	ε_T: bottom of layer (μm/m)		115	–	–	–	–
	NE_t		8.1 E+06	–	–	–	–
	$NE_{2t} = NE_t \times (1 - D_G)$		8.1 E+06	–	–	–	–
	ε_z: top of layer (μm/m)		–	–	259	200	152
	NE_{2z}		–	–	8.8 E+07	2.5 E+08	7.9 E+08
Step 2 - not bonded	ε_T: bottom of layer (μm/m)		142	–	–	–	–
	NE_t		2.8 E+06	–	–	–	–
	$NE_{2t} = NE_t \times (1 - D_G)$		2.8 E+06	–	–	–	–
	ε_z: top of layer (μm/m)		–	–	259	228	202
	NE_{2z}		–	–	8.8 E+07	1.5 E+08	2.5 E+08
Total	NE_1		4.5 E+07				
	Bonded	NE_2	8.1 E+06				
		NE_{Total}	5.3 E+07				
	Not bonded	NE_2	2.4 E+06				
		NE_{Total}	4.8 E+07				

Table 3A
Numerical calculation results considering GB3 as cracked (EGB3 = 2000 MPa) and geogrid placed between GB4_2 and GB3

Position 1: Geogrid between GB4_2 and GB3		Layer				
		GB4_2	GB3	GRH	GNT2	PF4
Step 1	ε_t: bottom of layer (μm/m)	54	78	–	–	–
	NE_{1t}	–	6.5 E+06	–	–	–
	N_G	3.6 E+08	–	–	–	–
	Damage D_G	1.8%	–	–	–	–
	ε_z: top of layer (μm/m)	–	–	169	130	110
	NE_{1z}	–	–	5.1 E+08	1.5 E+09	3.0 E+09
Step 2 - bonded	ε_t: bottom of layer (μm/m)	70	–	–	–	–
	NE_t	9.7 E+07	–	–	–	–
	$NE_{2t} = NE_t \times (1 - D_G)$	9.6 E+07	–	–	–	–
	ε_z: top of layer (μm/m)	–	–	167	134	118
	NE_{2z}	–	–	5.3 E+08	1.3 E+09	2.2 E+09
Step 2 - not bonded	ε_t: bottom of layer (μm/m)	86	–	–	–	–
	NE_t	3.5 E+07	–	–	–	–
	$NE_{2t} = NE_t \times (1 - D_G)$	3.4 E+07	–	–	–	–
	ε_z: top of layer (μm/m)	–	–	109	120	152

(*continued on next page*)

Table 3A (*continued*)

Position 1: Geogrid between GB4_2 and GB3			Layer				
			GB4_2	GB3	GRH	GNT2	PF4
	NE_{2z}		–	–	3.1 E+09	2.1 E+09	7.9 E+08
Total	NE_1		6.5 E+06				
	Bonded	NE_2	9.6 E+07				
		NE_{Total}	1.0 E+08				
	Not bonded	NE_2	3.4 E+07				
		NE_{Total}	4.1 E+07				

Table 4A
Numerical calculation results, considering GB3 as cracked (E_{GB3} = 2000 MPa) and geogrid placed between GB4_1 and GB4_2

Position 2: Geogrid between GB4_1 and GB4_2		Layer					
		GB4_1	GB4_2	GB3	GRH	GNT2	PF4
Step 1.1	ε_T: bottom of layer (μm/m)	10	54	78	–	–	–
	N_{G1_1}	1.6 E+12	–	–	–	–	–
	N_{G1_2}	–	6.6 E+07	–	–	–	–
	$NE_{1.1t}$	–	–	6.5 E+06	–	–	–
	Damage D_{G1_1}	0.0004%	–	–	–	–	–
	Damage D_{G1_2}	–	9.8%	–	–	–	–
	ε_z: top of layer (μm/m)	–	–	–	169	130	110
	$NE_{1.1z}$	–	–	–	5.1 E+08	1.5 E+09	3.0 E+09
Step 1.2	ε_T: bottom of layer (μm/m)	13	70	–	–	–	–
	N_{G2_1}	4.4 E+11	–	–	–	–	–
	NE_t	–	1.8 E+07	–	–	–	–
	Damage D_{G2_1}	0.005%	–	–	–	–	–
	$NE_{1.2t} = NE_t \times (1 - D_{G1\_2})$	–	1.6 E+07	–	–	–	–
	ε_z: top of layer (μm/m)	–	–	–	167	134	118
	$NE_{1.2z}$	–	–	–	5.3 E+08	1.3 E+09	2.2 E+09
Step 2 - bonded	ε_T: bottom of layer (μm/m)	115	–	–	–	–	
	NE_t	8.1 E+06	–	–	–	–	
	$NE_{2t} = NE_t \times (1 - D_{G1\_1} - D_{G2\_1})$	8.1 E+06	–	–	–	–	
	ε_z: top of layer (μm/m)	–	–	–	259	200	152
	NE_{2z}	–	–	–	8.8 E+07	2.5 E+08	7.9 E+08
Step 2 - not bonded	ε_T: bottom of layer (μm/m)	142	–	–	–	–	–
	NE_t	2.8 E+06	–	–	–	–	–
	$NE_{2t} = NE_t \times (1 - D_{G1\_1} - D_{G2\_1})$	2.8 E+06	–	–	–	–	–
	ε_z: top of layer (μm/m)	–	–	–	259	228	202
	NE_{2z}	–	–	–	8.8 E+07	1.5 E+08	2.5 E+08
Total	$NE_1 = NE_{1.1} + NE_{1.2}$	2.3 E+07					
	Bonded NE_2	8.1 E+06					
	Bonded NE_{Total}	3.1 E+07					
	Not bonded NE_2	2.8 E+06					
	Not bonded NE_{Total}	2.6 E+07					

Table 5A
Numerical calculation results, considering GB3 as disintegrated (E_{GB3} = 500 MPa) and geogrid placed between GB4_2 and GB3

Position 1: Geogrid between GB4_2 and GB3			Layer				
			GB4_2	GB3	GRH	GNT2	PF4
Step 1	ε_t: bottom of layer (μm/m)		–	–	–	–	–
	NE_{1t}		–	0.0 E+00	–	–	–
	ε_z: top of layer (μm/m)		–	–	167	134	118
	NE_{1z}		–	–	5.3 E+08	1.3 E+09	2.2 E+09
Step 2 - bonded	ε_t: bottom of layer (μm/m)		70	–	–	–	–
	NE_t		9.7 E+07	–	–	–	–
	ε_z: top of layer (μm/m)		–	–	167	134	118
	NE_{2z}		–	–	5.3 E+08	1.3 E+09	2.2 E+09
Step 2 - not bonded	ε_t: bottom of layer (μm/m)		86	–	–	–	–
	NE_t		3.5 E+07	–	–	–	–
	ε_z: top of layer (μm/m)		–	–	109	120	152
	NE_{2z}		–	–	3.1 E+09	2.1 E+09	7.9 E+08
Total	NE_1		0.0 E+00				
	Bonded	NE_2	9.8 E+07				
		NE_{Total}	9.8 E+07				
	Not bonded	NE_2	3.5 E+07				
		NE_{Total}	3.5 E+07				

Table 6A
Numerical calculation results, considering GB3 as disintegrated (E_{GB3} = 500 MPa) and geogrid placed between GB4_1 and GB4_2

Position 2: Geogrid between GB4_1 and GB4_2			Layer				
			GB4_1	GB4_2	GRH	GNT2	PF4
Step 1	ε_T: bottom of layer (μm/m)		13	70	–	–	–
	NE_{1t}		–	1.8 E+07	–	–	–
	N_G		4.4 E+11	–	–	–	–
	Damage D_G		0.004%	–	–	–	–
	ε_z: top of layer (μm/m)		–	–	129	103	95
	NE_{1z}		–	–	1.6 E+09	3.9 E+09	5.4 E+09
Step 2 - bonded	ε_T: bottom of layer (μm/m)		115	–	–	–	–
	NE_t		8.1 E+06	–	–	–	–
	$NE_{2t} = NE_t \times (1 - D_G)$		8.1 E+06	–	–	–	–
	ε_z: top of layer (μm/m)		–	–	259	200	152
	NE_{2z}		–	–	8.8 E+07	2.5 E+08	7.9 E+08
Step 2 - not bonded	ε_T: bottom of layer (μm/m)		142	–	–	–	–
	NE_t		2.8 E+06	–	–	–	–
	$NE_{2t} = NE_t \times (1 - D_G)$		2.8 E+06	–	–	–	–
	ε_z: top of layer (μm/m)		–	–	259	228	202
	NE_{2z}		–	–	8.8 E+07	1.5 E+08	2.5 E+08
Total	NE_1		1.8 E+07				
	Bonded	NE_2	8.1 E+06				
		NE_{Total}	2.6 E+07				
	Not bonded	NE_2	2.8 E+06				
		NE_{Total}	2.1 E+07				

Table 7A
Numerical calculation results, the corresponding number of admissible French standard axle load cycles and damage concerning the reference and reinforced structures

Example of application: thickness reduction		Layer				
		GB4	GB	GRH	GNT2	PF4
Reference Structure	ε_T: bottom of layer (μm/m)	–	53	–	–	–
	NE_t	–	4.5 E+07	–	–	–
	ε_z: top of layer (μm/m)	–	–	129	103	95
	NE_z	–	–	1.6 E+09	3.9 E+09	5.4 E+09
Total	NE	4.5 E+07				
Step 1 (h_{GB4}:12.1 cm)	ε_T: bottom of layer (μm/m)	26	66	–	–	–
	NE_{1t}	–	1.5 E+07	–	–	–
	N_G	1.4 E+10	–	–	–	–
	Damage D_G	0.1%	–	–	–	–
	ε_z: top of layer (μm/m)	–	–	165	129	115
	NE_{1z}	–	–	5.6 E+08	1.6 E+09	2.5 E+09
Step 2 - bonded (h_{GB4}: 12.1 cm)	ε_T: bottom of layer (μm/m)	89	–	–	–	
	NE_t	2.9 E+07	–	–	–	
	$NE_{2t} = NE_t \times (1 - D_G)$	2.9 E+07	–	–	–	
	ε_z: top of layer (μm/m)	–	–	222	176	145
	NE_{2z}	–	–	1.7 E+08	4.3 E+08	9.5 E+08
Total (h_{GB4}: 12.1 cm)	NE_1	1.5 E+07				
	NE_2	2.9 E+07				
	NE_{Total}	4.5 E+07				
Step 1 (h_{GB4}: 14 cm)	ε_T: bottom of layer (μm/m)	26	59	–	–	–
	NE_{1t}	–	2.6 E+07	–	–	–
	N_G	1.4 E+10	–	–	–	–
	Damage D_G	0.2%	–	–	–	–
	ε_z: top of layer (μm/m)	–	–	146	115	105
	NE_{1z}	–	–	9.3 E+08	2.5 E+09	3.6 E+09
Step 2 - not bonded (h_{GB4}: 14 cm)	ε_T: bottom of layer (μm/m)	98	–	–	–	
	NE_t	1.9 E+07	–	–	–	
	$NE_{2t} = NE_t \times (1 - D_G)$	1.9 E+07	–	–	–	
	ε_z: top of layer (μm/m)	–	–	132	142	170
	NE_{2z}	–	–	1.4 E+09	1.0 E+09	5.0 E+08
Total (h_{GB4}: 14 cm)	NE_1	2.6 E+07				
	NE_2	1.9 E+07				
	NE_{Total}	4.5 E+07				

References

Barksdale, R.D., 1991. Fabrics in Asphalt Overlays and Pavement Maintenance", National Cooperative Highway Research Program - Synthesis of Highway Practice 171. Transportation Res. Board, Washington DC, USA).

Burmister, D.M., 1943. The theory of stress and displacements in layered systems and applications to the design of airport runways. Highway Research Board 23, 126–148.

Button, J.W., Lytton, R.L., 2007. Guidelines for using geosynthetics with hot-mix asphalt overlays to reduce reflective cracking. Transport. Res. Rec. 2004 (1), 111–119.

Canestrari, F., Belogi, L., Ferrotti, G., Graziani, A., 2015. Shear and flexural characterization of grid-reinforced asphalt pavements and relation with field distress evolution. Mater. Struct. 48 (4), 959–975.

Chang, D.T.T., Ho, N.H., Chang, H.Y., Yeh, H.S., 1999. Laboratory and case study for geogrid-reinforced flexible pavement overlay. Transport. Res. Rec. 1687 (1), 125–130.

Corté, J.F., Goux, M.T., 1996. Design of pavement structures: the French technical guide. Transport. Res. Rec. 1539, 116–124.

Corté, J.F., 2001. Development and uses of hard-grade asphalt and of high-modulus asphalt mixes in France. Transportation Research Circular 503, 12–31.

Dykes, J.W., 1980. The use of fabric interlayers to retard reflective cracking. Proc. Assoc. Asphalt Paving Technol. 39, 354–368.

Freire, R.A., Di Benedetto, H., Sauzéat, C., Pouget, S., Lesueur, D., 2021. Crack propagation analysis in bituminous mixtures reinforced by different types of geogrids using digital image correlation. Construct. Build. Mater. 303 (124522) https://doi.org/10.1016/j.conbuildmat.2021.124522. ISSN 0950-0618.

Gaborit, P., 2015. Comportement thermo-mecanique de structures de chaussees bitumineuses. In: PhD Thesis. University of Lyon/ENTPE, France (in French).

Godard, E., Coppens, T., Doligez, D., 1993. Enrobé armé d'une grille en fibres de verre, comportement à la fatigue. Revue Générale Routes Aérodromes 713 (in French).

Godard, E., Van Rompu, J., Brissaud, L., Gileni, F., 2019. Renforcement des chaussées bitumineuses par grille de verre : bilan de 25 ans d'expérience, derniers développements. In: Proc. 12emes Rencontres Géosynthétiques, Nancy (in French).

Institut Des Routes, des Rues et des Infrastructures de Mobilité (IDRRIM), 2016. Diagnostic et conception des renforcements de chaussées. In: Paris : Centre d'Etudes et d'expertise sur les Risques, l'Environnement, la Mobilité et l'Aménagement (CEREMA) (in French).

Kumar, V.V., Saride, S., Zornberg, J.G., 2021. Fatigue performance of geosynthetic-reinforced asphalt layers. Geosynth. Int. 28 (6), 584–597.

Lesueur, D., Leguernevel, G., Riot, M., 2021. On the performance of geogrids for asphalt pavement reinforcement: laboratory evaluation and selected case studies. In: Proc. 7th Eurasphalt & Eurobitume Congress, Madrid paper 331.

Maintenance Technical Advisory Guide, 2009. Chapter 12: interlayers. In: Volume I; Flexible Pavement Preservation, second ed. California Dept. Transportation (Caltrans) Division of Maintenance.

Nguyen, M.L., Di Benedetto, H., Sauzéat, C., 2016. Crack propagation characterization of bituminous mixtures using four-point bending notched specimen test. Road Mater. Pavement Des. 17–1, 70–86. https://doi.org/10.1080/14680629.2015.1063535.

Nguyen, M.L., Hornych, P., Le, X.Q., Dauvergne, M., Lumière, L., Chazallon, C., Sahli, Mehdi, Mouhoubi, S., Doligez, D., Godard, E., 2021. Development of a rational design procedure based on fatigue characterisation and environmental evaluations of asphalt pavement reinforced with glass fibre grid. Road Mater. Pavement Des. 22 (Suppl. 1), S672–S689. https://doi.org/10.1080/14680629.2021.1906304.

Nguyen, M.L., Sauzéat, C., Di Benedetto, H., Tapsoba, N., 2013a. Validation of the Time-Temperature superposition principle for crack propagation in bituminous mixtures. Mater. Struct. 46 (7), 1075–1087. https://doi.org/10.1617/s11527-012-9954-7.

Nguyen, M.L., Sauzéat, C., Di Benedetto, H., Wendling, L., 2008. Investigation of cracking in bituminous mixtures with a 4 points bending test. In: Al-Qadi, Scarpas, Loizos (Eds.), Proceedings of the 6th Rilem Int. Conf. On Cracking in Pavement. Balkema Pub., Chicago, pp. 284–293. https://doi.org/10.1201/9780203882191.ch28.

Nguyen, M.L., Blanc, J., Kerzrého, J.P., Hornych, P., 2013b. Review of glass fibre grid use for pavement reinforcement and APT experiments at IFSTTAR. Road Mater. Pavement Des. 14 (Suppl. 1), 287–308.

Nguyen, M.L., Chazallon, C., Sahli, M., Koval, G., Hornych, P., Doligez, D., Godard, E., 2020. Design of reinforced pavements with glass fiber grids: from laboratory evaluation of the fatigue life to accelerated full-scale test. In: Accelerated Pavement Testing to Transport Infrastructure Innovation. Springer, Cham, pp. 329–338.

Olard, F., 2012. GB5 mix design: high-performance and cost-effective asphalt concretes by use of gap-graded curves and SBS modified bitumens. Road Mater. Pavement Des. 13 (Suppl. 1), 234–259.

Pereira, P., Pais, J., 2017. Main flexible pavement and mix design methods in Europe and challenges for the development of an European method. J. Traffic and Transpor. Engi (English Edition ume 4 (4), 316–346. https://doi.org/10.1016/j.jtte.2017.06.001. ISSN 2095-7564.

Polidora, J., Sobhan, K., Reddy, D.V., 2019. Effects of geosynthetic inclusions on the fatigue and fracture properties of asphalt overlays. In: Proceedings of the XVII ECSMGE-2019. Geotechnical Engineering foundation of the future, pp. 1–8.

Service d'Etudes Techniques des Routes et Autoroutes (SETRA), 1994. Laboratoire Central des Ponts et Chaussées (LCPC). In: Conception et dimensionnement des structures de chaussée, Guide technique", Paris : SETRA/LCPC (in French).

Smith, L.L., Gartner, W., 1962. Welded wire fabric reinforcement for asphaltic concrete. Highway Res. Board Bulletin 322.

Van Rompu, J., Godard, E., Brissaud, L., Loison, E., 2017. Procédé de renforcement d'enrobé Colgrill R: qualification des grilles en laboratoire et exemple de réalisation. Revue Générale des Routes et des Aménagements 944, 30–35 (in French).

Williams, E.G., 1954. Application of wire mesh reinforcement to asphaltic concrete pavement overlays. In: Highway Materials Res. Lab. Report. Lexington, KY, USA.